

Intense laser-induced recombination: The inverse above-threshold ionization process

S. X. Hu* and L. A. Collins†

Theoretical Division, Los Alamos National Laboratory, Los Alamos, New Mexico 87545, USA

(Received 6 February 2004; published 13 July 2004)

We investigated the recombination of electrons with ions in an ultrashort, intense laser pulse by numerically solving the time-dependent Schrödinger equation. The inverse above-threshold ionization (IATI) phenomenon, which shows the recombination probability peaked at specific energies of the injected electron wave packet, is explicitly elucidated. Furthermore, these IATI peaks which are separated by the laser photon energy also show up in processes of recombination to excited states.

DOI: 10.1103/PhysRevA.70.013407

PACS number(s): 34.50.Rk, 32.80.Wr, 34.80.Lx

I. INTRODUCTION

Radiative recombination, by which a continuum electron interacting with an ion or atom becomes bound through the release of a photon, has attracted considerable theoretical and experimental attention for almost three-quarters of a century. This sustained popularity stems from the many environments in which recombination plays a vital role. For example, recombination critically determines the energy and charge balance, as well as certain diagnostics, in many terrestrial and astronomical plasmas. Modeling of high-energy-density and fusion-energy (tokamak) devices, planetary and stellar atmospheres, and interstellar media relies heavily on a detailed knowledge of this mechanism. The advent of lasers added a new possibility, that of manipulating the outcome of the recombination process by tuning the laser field [1]. These early endeavors at laser-assisted recombination (LAR) employed weak fields to stimulate the emission of a photon at the driving frequency of the laser [2]. Several experimental groups have reported significant enhancements of recombination rates using either pulsed [3] or cw [4] lasers. Similar enhancements can also occur during the pulsing of the field within an ion trap [5]. This success has led to considerations of LAR for increasing the production of certain exotic species such as antihydrogen and positronium [6,7].

Subsequent experimental developments produced shorter pulse lengths and more intense laser fields, comparable in magnitude to the atomic binding. These intense field interactions introduced multiphoton processes, associated with the frequency of the driving laser, into the basic recombination mechanism, thereby further enriching the possibilities. Laser-assisted recombination also forms one component of the three-step process usually envisioned for high-order harmonic generation (HHG). In this case, the intense field first produces multiphoton ionization of an atom. In the second phase, the electron begins to tunnel through the potential created by the ion and the laser field. For particular orientations and strengths, this field may return the electron to the vicinity of the nucleus. At which point, as the third step, the electron may recombine and emit a high-energy photon. If

instead of recombining, the electron remains in the continuum and moves completely away from the core, we would obtain the standard above-threshold ionization (ATI) mechanism. Thus, recombination in an intense field can be viewed as the inverse of above-threshold ionization (IATI) much as photoionization forms the inverse of laser-free radiative recombination. The third step in HHG, which also occurs during LAR, attracts additional interest by providing a mechanism for the generation of attosecond pulses [8]. Therefore, a detailed description of LAR not only yields a better understanding of intense-field recombination but also of other associated processes.

In contrast to the case of *weak* LAR, the study of *intense* laser-induced multiphoton recombination of electrons and ions has only recently received attention [9–13], as opposed to its complementary process of ionization [14–19]. In addition, the past few years have witnessed an increasing interest in the related process of intense laser-assisted x-ray/electron-atom scattering [20–22]. The recent studies [9–13] of intense LAR have focused on the radiation spectrum (i.e., x-ray generation) and employed the strong-field approximation within a Keldysh-type formulation. These pioneering studies have mostly concentrated on the process of recombination directly into the atomic ground state with the contributions from the intermediate states neglected. In this paper, we consider an alternative approach by solving the full time-dependent Schrödinger equation (TDSE) for the electron-ion recombination in an ultrashort, intense laser pulse. Our TDSE solution includes in a consistent fashion all the separate processes discussed in the recent analysis [9–13]. Moreover, by solving the TDSE, we can examine the dynamical evolution of the recombined population and judge the importance of the intermediate states in the intense LAR processes. In particular, we are interested in the recombination dependence on the incident electron energy. To this end, we begin in the next section with a short exposition of the formalism and computational methods employed, followed by a section that presents our results with an accompanying discussion.

II. FORMULATION

As a representative system, we consider the interaction of a free electron with a proton in the presence of an intense laser field. A quantum-mechanical depiction of this process

*Email address: suxing@lanl.gov

†Email address: lac@lanl.gov

involves an electron wave packet, initially positioned at a distance R_0 from the nucleus with a momentum $p_0(E_k \equiv p_0^2/2)$, evolving according to a time-dependent Schrödinger equation of the form (atomic units [23])

$$i \frac{\partial \Psi(x,y|t)}{\partial t} = \left[-\frac{1}{2} \left(\frac{\partial^2}{\partial x^2} + \frac{\partial^2}{\partial y^2} \right) - \frac{1}{\sqrt{q_e + x^2 + y^2}} + xE_0 f(t) \cos(\omega t) \right] \Psi(x,y|t). \quad (1)$$

We have made the dipole approximation and considered linear polarization, which imparts a preferred direction in the case of an intense field that permits a reduction to a two-dimensional form. The laser pulse has a Gaussianlike envelope $[f(t) = \sin^2(\pi t/T)]$ with a duration T , a peak field strength of E_0 , and a frequency of $\omega(\lambda = 2\pi/\omega)$ with polarization along the x axis and propagation in the y direction. A two-dimensional soft-core potential [24] approximately describes the Coulomb attraction with the nucleus. In the absence of external fields, this potential supports a number of bound states n , designated by the wave function $\Phi_n(x,y)$. Selecting the screening parameter as $q_e = 0.63$ gives a lowest-energy level of $\varepsilon_1 = -0.5$ a.u., corresponding to the ground state of the hydrogen atom.

The initial state consists of a Gaussian wave packet at a distance R_0 (along x) from the nucleus with momentum p_0 , specifically,

$$\Psi(x,y | t=0) = N \exp \left[-\frac{(x+R_0)^2}{2\sigma_x^2} - \frac{y^2}{2\sigma_y^2} \right] e^{ip_0 x}, \quad (2)$$

where σ_x and σ_y represent the width in x and y directions, respectively, and N the normalization constant. Typically, we choose $\sigma_x = \sigma_y = 5a_B$ to produce a narrow momentum distribution. In order to maximize the recombination probability, we arrange for the electron wave packet to reach the nucleus at the peak laser intensity [$R_0 = p_0(T/2)$].

We solve the TDSE for the initial condition in Eq. (2) by applying a split-operator algorithm [25] in a spatial box of size $204.8 a_B \times 51.2 a_B$. Most cases employ a grid of 2048 points in the x dimension and 512 in the y dimension with step sizes $[\Delta_x = \Delta_y]$ of $0.1a_B$. This particular choice of grids stems from the kinetic energy propagation, which employs a fast Fourier transform that requires grids of 2^n points. The application of absorption edges [26] in each dimension significantly reduces reflection at the boundaries. We performed numerous sensitivity checks with respect to the coordinate ranges and step size. We found little dependence of the basic features on the extent of the box in x (e.g., $n_x = 4096$, $\Delta_x = 0.1a_B$) or the grid size (0.2 compared to $0.1a_B$). We did observe some dependence on the extent of the y box, especially for the low-energy collisions ($p_0 < 0.30$ a.u.). This arises from the greater spreading of the wave packet under these conditions. Good convergence though resulted between 512 and 1024 points.

We performed one TDSE calculation for each electron wave packet characterized by an initial momentum p_0 , and calculated the recombination probability $P_n(p_0|t)$ to a bound state Φ_n by projecting onto the total wave function

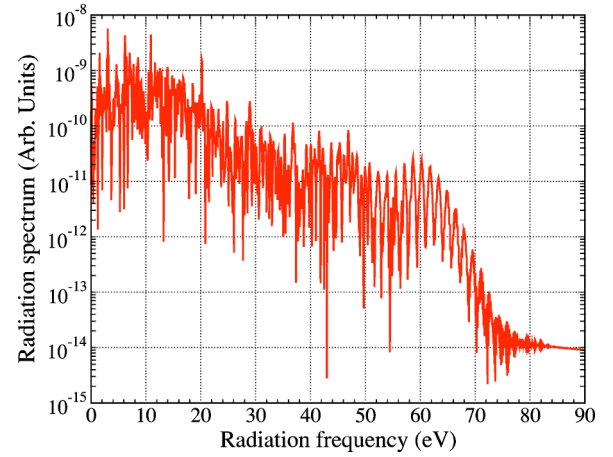


FIG. 1. (Color online) The radiation spectrum for the recombination process.

$$P_n(p_0|t) = \iint \Phi_n^*(x,y) \Psi(x,y|t) dx dy. \quad (3)$$

We continued the TD propagation beyond the termination of the laser interaction ($t > T$) to check that the final recombined populations in the eigenstates did not overlap the outgoing component of the wave packet.

III. RESULTS AND DISCUSSION

As suggested by earlier analytical studies [9–13], intense laser-induced recombination should generate x-ray radiation. Thus, as a first test of our procedure, we calculate the radiation spectrum by considering an initial electron wave packet with $p_0 = 0.5$ scattering from the model hydrogen potential in an intense (2×10^{14} W/cm²) laser field ($\lambda = 800$ nm; period = 2.67 fs) with a pulse duration of 50 fs. To reproduce these earlier studies, which considered only a purely periodical laser field, we have selected a pulse duration (~ 18 cycles) much longer than that for subsequent simulations. The calculated spectrum as displayed in Fig. 1 shows a radiation cutoff ($\hbar\omega_{\max}$) at ~ 60 eV, in very good agreement with the analytical prediction [9–13],

$$\hbar\omega_{\max} = E_k + I_p + 2U_p + 2\sqrt{2E_k U_p}, \quad (4)$$

with I_p , the ionization potential, and $U_p (= E_0^2/4\omega^2)$, the laser ponderomotive potential. Since our approach includes many recombination channels, such as to excited states, in addition to the direct transition to the ground state investigated in Refs. [9–13], we expect differences especially in the low frequency regime. However, the agreement in the high-frequency cutoff provides a general demonstration of our approach.

We now turn our attention to the dependence of the recombination process on the energy of the incident electron. Figure 2 shows the results in which an ultrashort ($T = 7.5$ fs; ~ 3 cycles), intense (10^{14} W/cm²) laser pulse at 800 nm (a Ti:sapphire laser) assists the electron-ion recombination. Figure 2(a) indicates the probability $P_0(p_0|T)$ at the end of the laser pulse of electron recombination into the ground state,

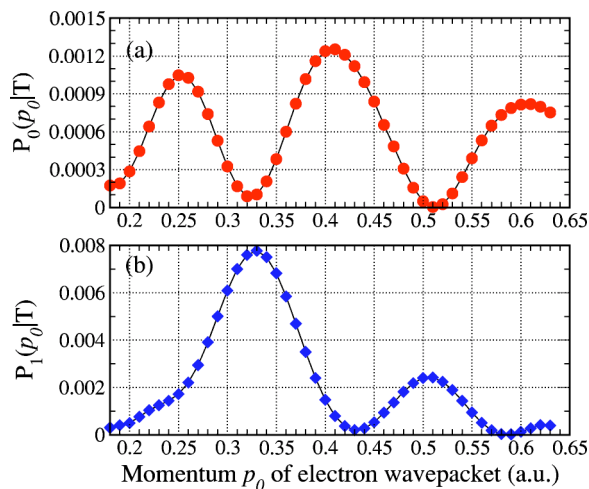


FIG. 2. (Color online) The intense laser-induced recombination probability $P_n(p_0|T)$ is plotted as a function of the initial momentum p_0 of the free-electron wave packet to: (a) the ground state and (b) the first excited state of a model hydrogen. The ultrashort laser ($\lambda=800$ nm) pulse has a Gaussianlike (\sin^2) temporal envelope with a duration of $T=7.5$ fs, and its peak intensity is equal to 10^{14} W/cm 2 .

as a function of the initial momentum p_0 of the free electron wave packet. We recall that each point in the plot corresponds to a solution of the TDSE for a specific p_0 . The most noticeable feature of the plot is the occurrence of recombination at specific momenta (energies) of the incident electron wave packet. The first peak, located at $p_0 \approx 0.25$ a.u., corresponds to the initial kinetic energy of $E_k \approx 0.85$ eV. Taking into account the ponderomotive upshift ($U_p \approx 5.82$ eV) of the ionization potential $I_p = 13.6$ eV, we find that the energy difference between the free electron and the ground state equals 20.27 eV. The ratio of this energy difference to the laser photon energy is very close to the integer 13 (≈ 20.27 eV/1.552 eV). Essentially, this implies that the intense laser-induced multiphoton recombination occurs as the inverse process of the above-threshold ionization in which the bound-state electron absorbs an integer number of laser photons, thereby generating photoelectron peaks in the continuum. Namely, an inverse ATI (IATI) peak will appear in the recombination spectrum, if the following resonance condition is satisfied:

$$E_k + I_p + U_p = n\hbar\omega. \quad (5)$$

This condition also coincides with the analytical formula for x-ray generation [9,13]. Once Eq. (5) is met, the electron emits a high-energy photon ($=n\hbar\omega$) and radiatively recombines to a bound state with ionization potential I_p . Returning to Fig. 2(a), we find the next recombination peak at $p_0 \approx 0.41$ a.u., which corresponds to $n=14$ and to a separation from the first peak approximately by one laser photon. However, the $n=15$ multiphoton recombination peak that should exist near $p_0 \approx 0.53$ a.u. does not appear, although the $n=16$ peak still follows. The disappearance of the $n=15$ peak may arise from destructive interference processes involving other bound states. Interestingly, a similar situation of miss-

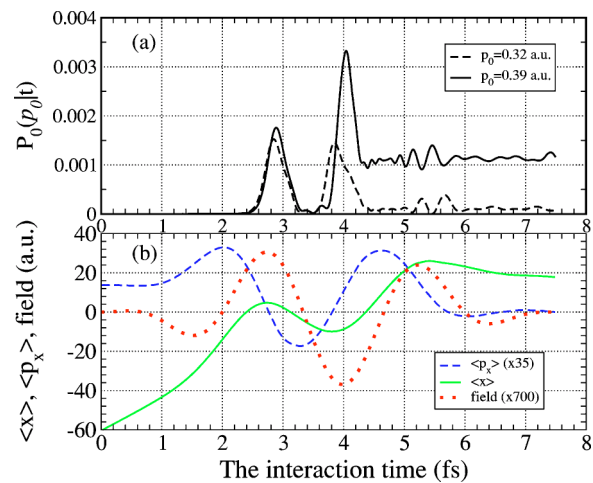


FIG. 3. (Color online) (a) The time evolution of the ground-state population during the entire pulse interaction and (b) the center-of-mass position $\langle x \rangle$ (solid green line) and momentum $\langle p_x \rangle$ 35; blue dashed line) for the two wave packets and the laser field envelope $E(t)$ ($\times 700$; red dotted line). The laser parameters are the same as those used in Fig. 2.

ing multiphoton peaks occurs in the normal ATI spectra [27].

Figure 2(b) shows the recombination into the first excited state P_1 . We also observe IATI peaks separated by the laser photon energy. Taking into account the ponderomotive shift ($U_p \sim 5.82$ eV) for the loosely bound first excited state ($I_p \approx 5$ eV), we determine that the first IATI peak at $p_0 \sim 0.33$ a.u. corresponds to an eight-photon process ($n=8$). The following two peaks account for $n=9$ and $n=10$. Comparing Figs. 2(a) and 2(b), we find that the probability of recombination to the first excited state dominates that to the ground state by a factor of 8. This seems reasonable since for a specific momentum p_0 , recombination to the first excited state represents a lower-order IATI process, $n=8$ compared to $n=13$. Recombination to excited states has generally been considered less important than to the ground level and has been neglected in other studies [9–13]. However, these findings indicate that in some situations these processes may have rather profound effects on the overall recombination.

From the TDSE solution, we can trace the details of the recombination dynamics. In Fig. 3(a) we display the evolution of the population in the ground state $P_0(p_0|t)$ during the entire interaction with the laser pulse for two special cases $p_0=0.32$ (dashed line) and 0.39 a.u. (solid line). The final recombination probabilities associated with these two momenta correspond respectively to local minimum and nearby maximum in Fig. 2(a). We plot in Fig. 3(b) the laser field $E(t)=E_0 \cos(\omega t)f(t)$, as well as the expectation value of the position ($\langle x \rangle$) and momentum ($\langle p_x \rangle$) along the x axis for a wave packet with $p_0=0.39$ a.u. Starting from a position along the negative x axis, the electron accelerates towards the nucleus under the influence of the attractive Coulomb-like potential and the laser field. Around a time of 2 fs, the field reserves and presents the electron with a repulsive barrier. The electron in turn begins to slow in the vicinity of the nucleus. As this occurs, the ground state population grows as recombination becomes very effective. The field reaches a

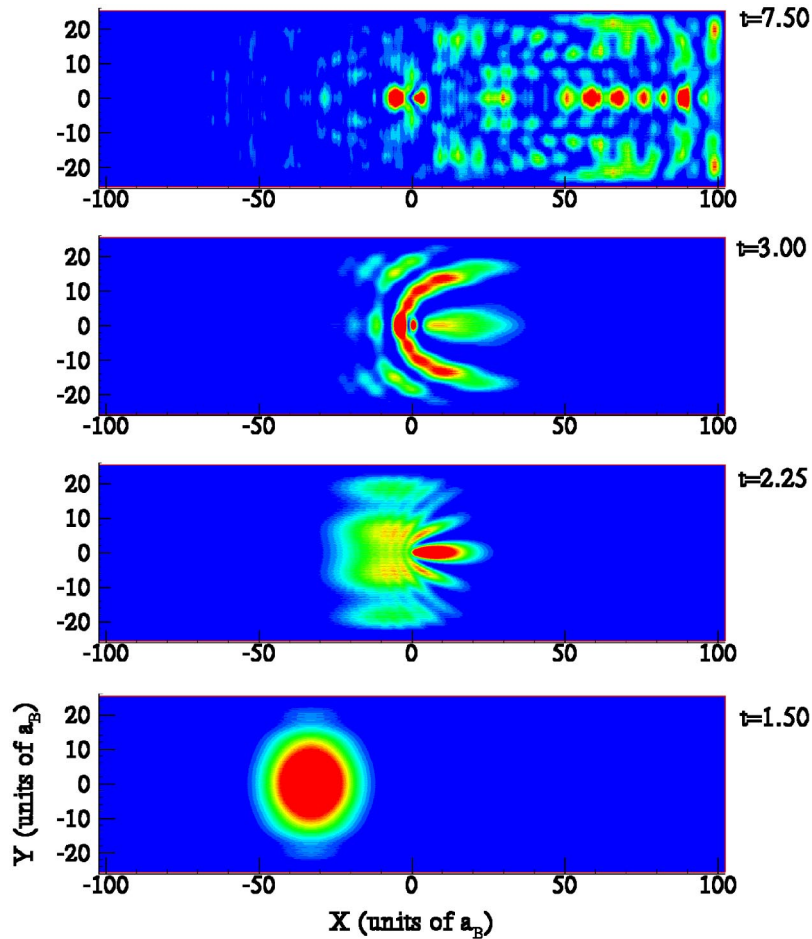


FIG. 4. (Color online) Contour displays of the probability density $|\Psi(x,y)|^2$ as a function of time for $p_0=0.39$ a.u. and the laser parameters of Fig. 3. Maximum intensity [dark gray (red)] set to a probability of 0.001 for times of 1.5, 2.25, and 3.00 fs and of 0.0005 for 7.5 fs.

maximum (~ 2.7 fs), completely stopping the electron ($\langle p_x \rangle \approx 0$) and reversing its direction. At this point, we observe a large recombination peak indicated in Fig. 3(a). The recombination peak appearing near the field maxima and $\langle p_x \rangle \approx 0$ has an analog in the tunneling process of normal ATI, in which the bound-electron wave packet tunnels through the intense laser-dressed atomic potential barrier as the laser field reaches its maxima. However, since ionization processes also occur within the field, most of this population is lost as the electron traverses the potential well. The field again changes sign (~ 3.3 fs), driving the packet back across the well and leading to another maximum around 4 fs in the recombination. This recombination-reionization process recurs for the remaining duration of the pulse. If the initial kinetic energy ($p_0^2/2$) satisfies the multiphoton resonance condition [Eq. (5)], then the ground-state population remains elevated through the duration of the pulse as illustrated for $p_0=0.39$ a.u. (solid line). On the other hand, if not, the ground-state population drops and remains at a small value as shown by the dashed line ($p_0=0.32$ a.u.). The examination of averaged quantities along the x direction provides general insight into the IATI mechanism; however, it can mask the complicated intricacies of the full TD process.

To this end, we examine the temporal evolution of the probability density $|\Psi(x,y)|^2$. Figure 4 depicts representative events over the full duration of the pulse and displays intensities set to two different maximums of the probability: 0.001 for the first three times and 0.0005 for 7.5 fs. This adjustment in correspondence between the color template and the probability provides the greatest contrast and illuminates the major features. At early times ($t=1.50$ fs), the packet assumes its initial free Gaussian form. By $t=2.25$ fs, the field has reversed causing the packet to slow. Considerable recombination has occurred as evidenced by the intense pattern in the vicinity of the nucleus. In addition, a part of the pack has already reflected from the field and moved back across the center. The third panel corresponds to a weakening field that allows some of the probability to stream out in the positive x direction. In the final panel ($t=7.5$ fs), the pulse has died, and the pieces, arising from multiple field reversals and close nuclear encounters, move out in the remaining Coulomb potential. We have, in addition to lowering the maximum probability presented, decreased the lower bound to depict the wealth of detail that arises during the complete pulse duration. As a further example, we display a short time sequence in Fig. 5 and a surface plot in Fig. 6.

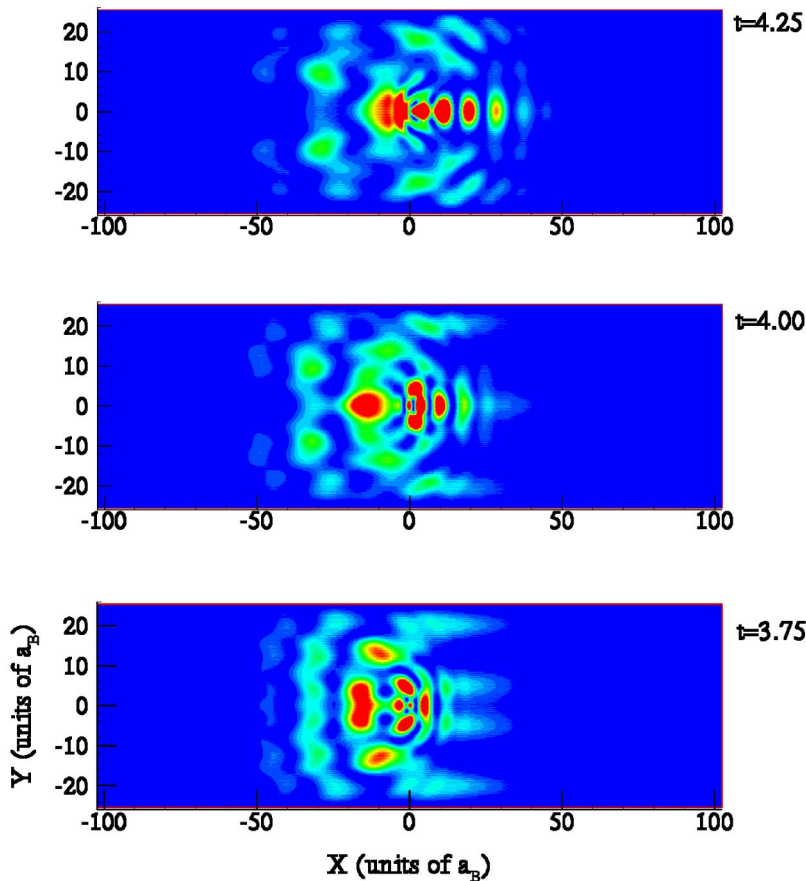


FIG. 5. (Color online) The same as Fig. 4 but at different times.

We now examine the effects of the laser intensity on the IATI process. Figures 7(a) and 7(b) show the recombination probability to the *ground state* for laser intensities of $I=1.3$ and 2×10^{14} W/cm², respectively, with the other laser parameters the same as for Fig. 2. IATI peaks similar to those of Fig. 2(a) clearly appear with shifted positions due to the intensity dependence of U_p . In Fig. 7(a) the first peak at $p_0 \approx 0.20$ a.u. corresponds to the $n=14$ multiphoton process, while the peak at $p_0 \approx 0.25$ a.u. in Fig. 7(b) represents $n=17$. The positions of the peaks basically fulfill the multiphoton resonance condition of Eq. (5). By comparing to Fig. 2(a), we find a distinct enhancement in the recombination probability with increasing laser intensity.

Figures 7 and 2(a) yield another interesting trend, namely that the IATI peak amplitudes become larger for high-order processes. For example, in Fig. 7(b) the $n=18$ (at p_0

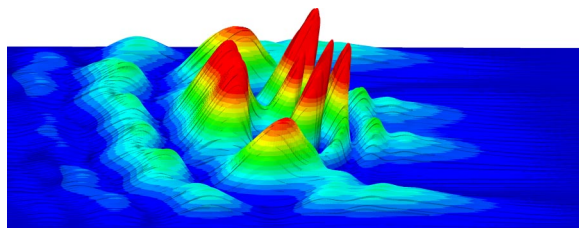


FIG. 6. (Color online) The surface plot of the probability density at $t=3.75$ fs.

~ 0.37 a.u.) and $n=19$ (at $p_0 \sim 0.51$ a.u.) processes have larger probabilities than the $n=17$. This seems at first counterintuitive since generally for a given set of parameters, the higher the order, the less likely the occurrence. However, we can understand this trend, at least qualitatively, by considering partial channel closings. During a laser cycle, the additional quivering energy of electrons in a laser field varies instantaneously with the field, ranging from zero to $2U_p$. We

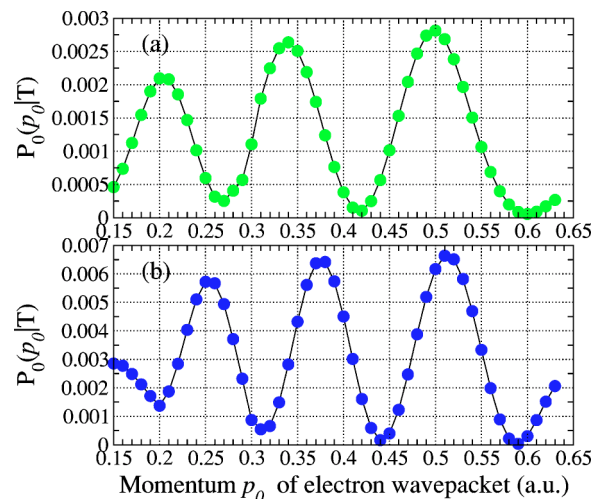


FIG. 7. (Color online) Similar to Fig. 2(a) but for different laser intensities: (a) $I=1.3 \times 10^{14}$ W/cm² and (b) $I=2 \times 10^{14}$ W/cm².

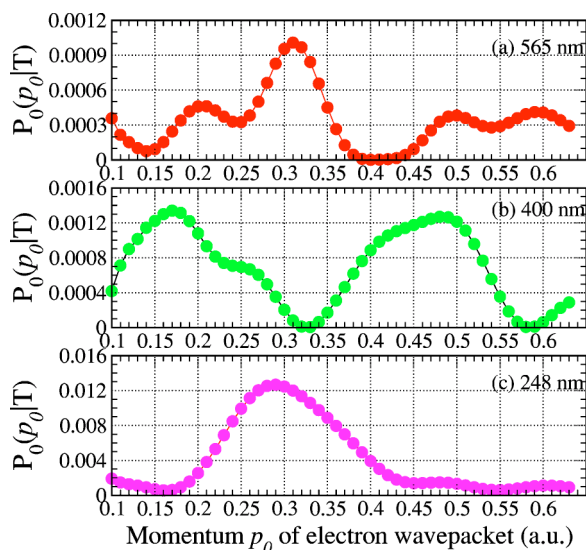


FIG. 8. (Color online) The IATI spectrum for different driving laser wavelengths: (a) $\lambda=565$ nm, (b) $\lambda=400$ nm, and (c) $\lambda=248$ nm. The laser pulse has a peak intensity of 10^{14} W/cm 2 , with the same duration of $T=7.5$ fs.

start with the field at zero and a particular set $\{n\}$ of allowed multiphoton recombination energies ($n\hbar\omega=E_k+I_p$). As the field rises, the lower-order processes become disallowed according to the energy conservation condition. With decreasing intensity, these channels again open to permit recombination. The ponderomotive potential, which represents the laser-period averaged quivering energy of an electron, acts as an effective additional ionization barrier. The higher the order, the less closure occurs during the laser cycle. The magnitude of the recombination peaks results then from a competition between the order of the process and the degree to which the channel closes during the pulse. Interestingly, this kind of phenomenon has been noticed and observed in the normal ATI spectra [28].

Finally, we check the dependence of the IATI process on the driving laser wavelength. Results for the recombination to the ground state appear in Fig. 8 for (a) $\lambda=565$ nm ($\hbar\omega=2.2$ eV), (b) $\lambda=400$ nm (3.1 eV), and (c) $\lambda=248$ nm (5.0 eV) for a peak laser intensity of $I=10^{14}$ W/cm 2 with a duration of $T=7.5$ fs. Generally, the IATI peaks, separated by the photon energy of the driving laser, still arise in the recombination spectra for different laser wavelengths. However, some subtle differences exist. For example, in Fig. 8(a), as expected, we have IATI peaks for the $n=8$ and $n=9$ processes at momenta of 0.31 and 0.50 a.u., respectively. However, we also discover additional peaks at $p_0\approx 0.20$ and ≈ 0.60 a.u. that do not correspond to any direct recombina-

tion process to the ground state. In addition, for the case of $\lambda=400$ nm, indicated by Fig. 8(b), we recover not only the $n=5$ ($p_0=0.17$ a.u.) and $n=6$ ($p_0\approx 0.50$ a.u.) IATI peaks, but also bumps at around $p_0\approx 0.25$ and ≈ 0.42 a.u. We attribute these extra structures to *indirect* process by which the free electron first recombines into an excited level with the subsequent laser deexcitation to the ground state. Its counterpart in normal ATI evinces itself as the excitation of intermediate states [29]. Additional support for this view comes from examining at $\lambda=400$ nm the population in the second excited state, which displays distinct dips for p_0 around 0.25 and 0.42 a.u. We note that these indirect recombinations appear more significant for short-wavelength lasers, as compared to the results for 800 nm (indicated in Figs. 2 and 7). Figure 8(c) examines the case for a 248 nm laser with a ponderomotive component $U_p\approx 0.54$ eV much smaller than either the ionization potential or the laser photon energy ($\hbar\omega=5$ eV). We identify the dominant peak at $p_0\approx 0.29$ a.u. with the *direct* three-photon recombination process. Comparing the magnitudes of recombination probabilities in Fig. 8, we conclude that short-wavelength lasers generally favor IATI since lower-order processes dominate.

IV. CONCLUSION

We have investigated the recombination, induced by an ultrashort and intense laser pulse, of free-electron wave packets into atomic bound states through numerically solving the time-dependent Schrödinger equation. The recombination peaks appear at specific incident electron energies, separated by the photon energy of the driving laser. This phenomenon is essentially the inverse to the normal ATI process. In addition to direct recombination to the atomic ground state, we also observed IATI features in the spectra of recombination to excited states. These excitation mechanisms, often neglected, can have significant effects on the total recombination process. Many of the phenomena associated with standard ATI have counterparts in recombination. For example, certain IATI peaks appear suppressed and interlopers, not associated with direct multiphoton transitions, arise. These features probably originate from indirect processes involving intermediate transition to excited states. Finally, we studied the behavior of the IATI structures as a function of intensity and wavelength. The degree of recombination rises for shorter wavelengths since these favor lower-order processes.

ACKNOWLEDGMENTS

This work was performed under the auspices of the U.S. Department of Energy through the Los Alamos National Laboratory under Contract No. W-7405-ENG-36.

- [1] Y. Hahn, Rep. Prog. Phys. **60**, 691 (1997).
 [2] L. A. Rivlin, Kvantovaya Elektron. (Moscow) **6**, 594 (1979) [Sov. J. Quantum Electron. **9**, 353 (1979)]; F. H.M. Faisal *et al.*, J. Phys. B **14**, L569 (1981); B. Ritchie, Phys. Rev. A **30**,

- 1849 (1984); R. Neumann *et al.*, Z. Phys. A **313**, 253 (1983); E. E. Fill, Phys. Rev. Lett. **56**, 1687 (1986).
 [3] U. Schramm *et al.*, Phys. Rev. Lett. **67**, 22 (1991).
 [4] F. B. Yousif *et al.*, Phys. Rev. Lett. **67**, 26 (1991).

- [5] F. Robicheaux and M. S. Pindzola, *Phys. Rev. Lett.* **79**, 2237 (1997); C. Wesdorp, F. Robicheaux, and L. D. Noordam, *Phys. Rev. Lett.* **84**, 3799 (2000); *Phys. Rev. A* **64**, 033414 (2001).
- [6] A. Wolf, *Hyperfine Interact.* **76**, 189 (1993).
- [7] R. J. Whitehead, J. F. McCann, and I. Shimamura, *Phys. Rev. A* **64**, 023401 (2001); J. S. Cohen, *Phys. Rev. A* **67**, 017401 (2003).
- [8] M. Drescher *et al.*, *Science* **291**, 1923 (2001); P. M. Paul *et al.*, *ibid.* **292**, 1689 (2001).
- [9] M. Yu. Kuchiev and V. N. Ostrovsky, *Phys. Rev. A* **61**, 033414 (2000); *J. Phys. B* **34**, 405 (2001).
- [10] F. Ehlötzky, A. Jaroń, and J. Z. Kamiński, *Phys. Rep.* **297**, 63 (1998).
- [11] A. Jaroń, J. Z. Kamiński, and F. Ehlötzky, *Phys. Rev. A* **61**, 023404 (2000); **63**, 055401 (2001).
- [12] E. A. Nersesov, S. V. Popruzhenko, D. F. Zaretsky, W. Becker, and P. Agostini, *Phys. Rev. A* **64**, 023419 (2001).
- [13] D. B. Milošević and F. Ehlötzky, *Phys. Rev. A* **65**, 042504 (2002).
- [14] P. Agostini *et al.*, *Phys. Rev. Lett.* **42**, 1127 (1979).
- [15] R. R. Freeman *et al.*, *Phys. Rev. Lett.* **59**, 1092 (1987).
- [16] M. Protopapas, C. H. Keitel, and P. L. Knight, *Rep. Prog. Phys.* **60**, 389 (1997).
- [17] T. Brabec and F. Krausz, *Rev. Mod. Phys.* **72**, 545 (2000).
- [18] C. J. Joachain, M. Dörr, and N. Kylstra, *Adv. At., Mol., Opt. Phys.* **42**, 225 (2000).
- [19] W. Becker *et al.*, *Adv. At., Mol., Opt. Phys.* **48**, 35 (2002).
- [20] N. L. Manakov, A. F. Starace, A. V. Flegel, and M. V. Frolov, *JETP Lett.* **76**, 258 (2002).
- [21] D. B. Milošević and A. F. Starace, *Phys. Rev. Lett.* **81**, 5097 (1998).
- [22] L. B. Madsen, J. P. Hansen, and L. Kocbach, *Phys. Rev. Lett.* **89**, 093202 (2002).
- [23] Energy in units of Hartrees ($H=27.2$ eV); length in units of Bohr ($a_B=0.052918$ nm); and time in units of 0.0242 fs.
- [24] J. Javanainen, J. H. Eberly, and Q. Su, *Phys. Rev. A* **38**, 3430 (1988); J. H. Eberly, Q. Su, and J. Javanainen, *Phys. Rev. Lett.* **62**, 881 (1989).
- [25] M. D. Feit, J. A. Fleck, Jr., and A. Steiger, *J. Comput. Phys.* **47**, 412 (1982).
- [26] J. L. Krause, K. J. Schafer, and K. C. Kulander, *Phys. Rev. A* **45**, 4998 (1992); S. X. Hu and Z. Z. Xu, *Phys. Rev. A* **56**, 3916 (1997).
- [27] R. R. Jones, *Phys. Rev. Lett.* **74**, 1091 (1995); R. Kopold and W. Becker, *J. Phys. B* **32**, L419 (1999); R. Kopold, W. Becker, and M. Kleber, *Opt. Commun.* **179**, 39 (2000); G. G. Paulus, F. Grasbon, and H. Walther, *J. Mod. Opt.* **50**, 343 (2003).
- [28] P. H. Bucksbaum *et al.*, *Phys. Rev. Lett.* **56**, 2590 (1986); *J. Opt. Soc. Am. B* **4**, 760 (1987); B. Borca *et al.*, *Phys. Rev. Lett.* **87**, 133001 (2001); R. Kopold *et al.*, *J. Phys. B* **35**, 217 (2002).
- [29] P. Hansch, M. A. Walker, and L. D. VanWoerkom, *Phys. Rev. A* **57**, R709 (1998); S. X. Hu, W. X. Qu, and Z. Z. Xu, *Appl. Phys. Lett.* **73**, 2552 (1998).